PHYSICAL REVIEW B VOLUME 21, NUMBER 4 15 FEBRUARY 1980

Uniaxial-stress dependence of the first-order Raman spectrum of rutile. I. Experiments

P. Merle, J. Pascual,* J. Camassel, and H. Mathieu

Centre d'Etudes d'Electronique des Solides,† *Université des Sciences et Techniques du Languedoc, 34060 Montpellier-Cedex, France*

(Received 14 May 1979)

We report an investigation of the uniaxial-stress dependence of the first-order Raman spectrum of rutile (TiO_2). We find a normal-mode behavior, characterized by an increase in the phonon frequency versus uniaxial compression, for the two Raman modes Γ_1 (A_{1g}) and Γ_5 (E_g). We deduce two deformation potentials for Γ_1 (in unit of cm^{-1}): $a_1 = -610\ cm^{-1}$, $b_1 = -820\ cm^{-1}$ and four deformation potentials for Γ_5 (doubly degenerate mode): $a_5 = -1170\ cm^{-1}$, $b_5 = -1840\ cm^{-1}$, $c_5 = +35\ cm^{-1}$, and $d_5 = -230\ cm^{-1}$. We find less classical results for Γ_3 (B_{1g}): the phonon frequency increases for uniaxial stress parallel to $\vec{c}$ but decreases for uniaxial stress parallel to $\vec{a}$ ([100] direction) or parallel to $\vec{a}'$ ([110] direction). The corresponding deformation potentials are $a_3 = +620\ cm^{-1}$ and $b_3 = +330\ cm^{-1}$. Within experimental error, all phonon energies displace linearly versus deformation.

I. INTRODUCTION

The lattice vibration spectrum of rutile (TiO_2) is now fairly well understood. Comprehensive studies of Raman[1] and infrared[2] spectra have been published, and quite recently neutron[3] and Brillouin[4] scattering experiments have been performed. On the theoretical side a variety of models have been given, of which the most successful is an analysis of the dispersion data in terms of a shell model with tensor forces.[3] Concerning the Raman modes, the influence of hydrostatic perturbations such as temperature[5] and pressure[5,6] has been studied. Both reveal a softening of the low-frequency Γ_3 (B_{1g}) mode: The frequency decreases with decreasing internuclear distances. This behavior has been viewed[7] as indicative of a definite phase transition from the tetragonal rutile structure (D_{4h}^{14}) to the orthorhombic structure of $CaCl_2$ (D_{2h}^{12}). Since, in this case, the orthorhombic distortion would presumably be rather small (~2%; see Ref. 8), it can be easily achieved by applying a large uniaxial compression ($X \sim 17$ kbar) along one of the crystal's a axes. If we suppose that the Γ_3 mode is indeed especially sensitive to this stress configuration, we can expect to find a nonlinear behavior of the Γ_3 (B_{1g}) mode at 143 cm^{-1} and of the Γ_1 (A_{1g}) mode at 612 cm^{-1}. Indeed both modes, which achieve the same Γ_1 symmetry in the D_{2h} point group, should couple strongly. Such stress-induced couplings have been already reported for electronic energy levels in TiO_2 (Ref. 9) and Raman modes in paratellurite,[10] but were not found in a previous uniaxial-stress experiment of the Raman modes of rutile.[11] Finally, in the work of Ref. 11, which was restricted to rather low pressures (~3.5 kbar) and to configurations $\vec{X}\parallel\vec{c}$ and $\vec{X}\parallel\vec{a}$, no deformation potentials for phonons were deduced and the splitting of the doubly degenerate Γ_5 (E_g) mode was not resolved.

In this paper we investigate the stress dependence of the main Raman modes in configurations $\vec{X}\parallel\vec{c}$, $\vec{X}\parallel\vec{a}$, and $\vec{X}\parallel\vec{a}'$. In Sec. II we briefly set the theoretical background needed to analyze the data. In Sec. III we give the experimental details. In Sec. IV we present the results obtained with uniaxial stress ranging up to 10 kbar in the [001] direction ($\vec{c}$ axis), 6 kbar in the [100] direction ($\vec{a}$ axis), and last, 12 kbar in the [110] direction ($\vec{a}'$ axis). We separate all deformation potentials which combine to give the stress dependence of a given phonon. We get two deformation potentials (a_1, b_1 and a_3, b_3) for the nondegenerate modes Γ_1 (A_{1g}) and Γ_3 (B_{1g}), and four deformation potentials (a_5, b_5, c_5, d_5) for the doubly degenerate mode Γ_5 (E_g).

Discussing the experimental data, we show that the "soft" mode Γ_3, while weakly sensitive for a uniaxial stress directed along the crystal c axis, apparently stiffens versus pressure. This conclusion disagrees with the result of a previous paper[11] in which it was found that the pressure derivative obtained for Γ_3 under uniaxial stress parallel to $\vec{c}$ was small but positive. However, in both cases, the pressure coefficients reported are very small and the softening observed under hydrostatic conditions comes from the strong negative shifts observed when the force is either parallel to $\vec{a}$ or parallel to $\vec{a}'$. Finally, we show that there is no stress-induced coupling between Γ_1 and Γ_3 which would corroborate a special sensitivity of TiO_2 to the orthohombic distortion when $\vec{X}\parallel\vec{a}$. In the following paper, a model calculation for the deformation potentials of phonons in the rutile structure will be presented. It shows that the soft-mode behavior of the Γ_3 Raman mode comes directly from the atomic displacements associated with pure rotations of the oxygen atoms around

© 1980 The American Physical Society

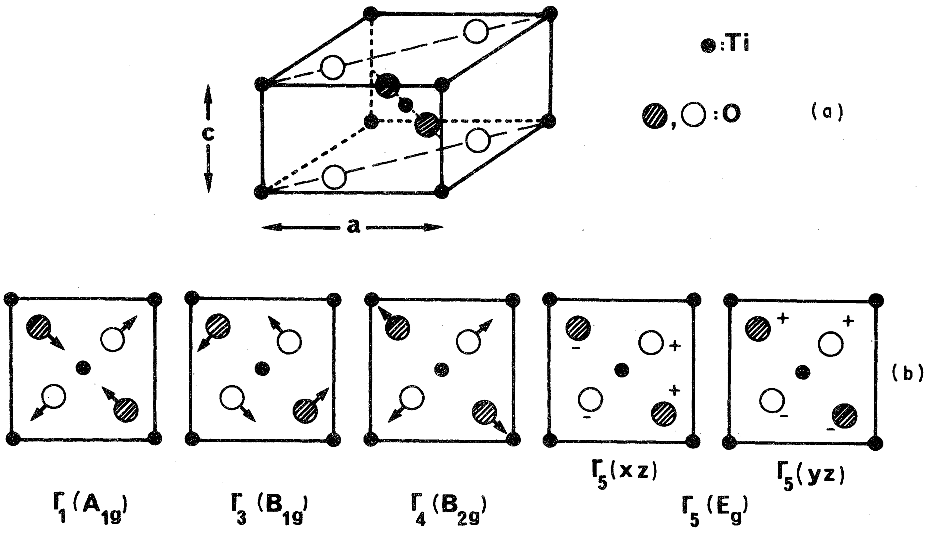

FIG. 1. (a) Tetragonal unit cell of rutile, (b) atomic displacements of atoms associated with vibrations Γ_1, Γ_3, Γ_4, and Γ_5.

the central titanium atom. The stress-induced change in the bond-bending constants, which happens in this case, accounts for the softening experimentally found under hydrostatic conditions.

II. THEORETICAL BACKGROUND

The tetragonal unit cell of rutile is shown in Fig. 1(a) (point-group symmetry D_{4h}). It contains six atoms (two formula units) which give a total of 18 phonon branches. Among them, three are acoustical branches: Γ point symmetry $\Gamma_{2'}(A_{2u}) + \Gamma_{5'}(E_u)$. The 15 remaining branches give the zone-center optical phonons

$$\Gamma_1(A_{1g}) + \Gamma_2(A_{2g}) + \Gamma_3(B_{1g}) + \Gamma_4(B_{2g}) + \Gamma_5(E_g) + \Gamma_{2'}(A_{2u}) + 2\Gamma_{3'}(B_{1u}) + 3\Gamma_{5'}(E_u) .$$

All Γ_5 and $\Gamma_{5'}$ modes are doubly degenerate. Modes of symmetry $\Gamma_{2'} + \Gamma_{5'}$ are infrared active while three modes $(\Gamma_2 + 2\Gamma_{3'})$ are silent. Finally, modes of symmetry Γ_1, Γ_3, Γ_4, and Γ_5 are Raman active. This is summarized in Table I, where we list also some useful basis functions. The displacement of atoms associated with the four Raman-active modes is shown in Fig. 1(b).

Associated with each Raman-active mode is a scattering tensor α_{ij}. In order to see experimentally one given component, one has to arrange the scattering geometry in such a way that the incident light is polarized in the i direction while the scattered light is analyzed in the j direction. On the other hand, since it is more convenient to refer the direction of polarization to the sample geometry, we introduce two sets of scattering tensors.

The first one refers to the crystallographic directions and corresponds to a rectangular cut of the sample ($\vec{x} \parallel \vec{a}$, $\vec{y} \parallel \vec{a}$, $\vec{z} \parallel \vec{c}$). The second corresponds to a 45° cut of the sample ($\vec{x}' \parallel \vec{a}'$, $\vec{y}' \parallel \vec{a}'$, $\vec{z}' \parallel \vec{c}$). It is used when the uniaxial stress is directed along a [110] direction (a' axis). Both

TABLE I. Phonon symmetries of rutile together with their infrared (ir) or Raman activity. Also listed are some basis functions of the corresponding irreducible representations.

Phonon mode of rutile (D_{4h})	Activity	Basis functions of the irreducible representations	
Γ_1 (A_{1g})	Raman	$f_0 = x^2 + y^2$, $\psi_0 = z^2$	$f'_0 = \psi_A^2 + \psi_B^2$, $\psi'_0 = f_1^2$
Γ_2 (A_{2g})	silent mode	R_z	
Γ_3 (B_{1g})	Raman	$f_1 = x^2 - y^2$	$f'_1 = \psi_A^2 - \psi_B^2$
Γ_4 (B_{2g})	Raman	$f_2 = xy$	$f'_2 = \psi_A \psi_B$
Γ_5 (E_g)	Raman	$\psi_A = zx$, $\psi_B = zy$	
Γ'_2 (A_{2u})	ir	z	
Γ'_3 (B_{1u})	silent		
Γ'_5 (E_u)	ir	x, y	

TABLE II. Polarizability tensors of the Raman-active modes of rutile for the rectangular and 45° cuts. Please note the apparent change in selection rules which appears between the Γ_3 (B_{1g}) and Γ_4 (B_{2g}) modes, respectively.

Rectangular cut ($\vec{x}\parallel\vec{a}$; $\vec{y}\parallel\vec{a}$; $\vec{z}\parallel\vec{c}$)			45° cut ($\vec{x}'\parallel\vec{a}'$; $\vec{y}'\parallel\vec{a}'$; $\vec{z}'\parallel\vec{c}$)	
Γ_1 (A_{1g})		$\begin{pmatrix} a & 0 & 0 \\ 0 & a & 0 \\ 0 & 0 & b \end{pmatrix}$		$\begin{pmatrix} a & 0 & 0 \\ 0 & a & 0 \\ 0 & 0 & b \end{pmatrix}$
Γ_3 (B_{1g})		$\begin{pmatrix} c & 0 & 0 \\ 0 & -c & 0 \\ 0 & 0 & 0 \end{pmatrix}$		$\begin{pmatrix} 0 & c & 0 \\ c & 0 & 0 \\ 0 & 0 & 0 \end{pmatrix}$
Γ_4 (B_{2g})		$\begin{pmatrix} 0 & d & 0 \\ d & 0 & 0 \\ 0 & 0 & 0 \end{pmatrix}$		$\begin{pmatrix} -d & 0 & 0 \\ 0 & d & 0 \\ 0 & 0 & 0 \end{pmatrix}$
Γ_5 (E_g)	Γ_5 (xz)	$\begin{pmatrix} 0 & 0 & e \\ 0 & 0 & 0 \\ e & 0 & 0 \end{pmatrix}$	Γ_5 ($x'z$)	$\begin{pmatrix} 0 & 0 & e \\ 0 & 0 & 0 \\ e & 0 & 0 \end{pmatrix}$
	Γ_5 (yz)	$\begin{pmatrix} 0 & 0 & 0 \\ 0 & 0 & e \\ 0 & e & 0 \end{pmatrix}$	Γ_5 ($y'z$)	$\begin{pmatrix} 0 & 0 & 0 \\ 0 & 0 & e \\ 0 & e & 0 \end{pmatrix}$

series of tensors are listed in Table II. It is interesting to note the change in selection rules which happens between Γ_3 and Γ_4, depending on the representation.

Under application of a static uniaxial compression X, the crystal deforms and reduces to a generally lower symmetry point group. All the symmetry elements of the new point group are common to both the unstrained crystal and the strain ellipsoid. For instance, a stress directed along the fourfold $\vec{c}$ axis leaves the tetragonal symmetry unchanged, while a stress directed along the twofold $\vec{a}$ or $\vec{a}'$ axis lowers the symmetry to $D_{2h}(x)$ and $D_{2h}(x')$, respectively. In Table III we list the corresponding compatibility relations. They show that the stress-induced change in symmetry results: (i) in a splitting of the doubly degenerate Γ_5 mode for both $\vec{X}\parallel\vec{a}$ and $\vec{X}\parallel\vec{a}'$; (ii) in stress-induced couplings of modes Γ_1 (Γ_2) with Γ_3 (Γ_4) when $\vec{X}\parallel\vec{a}$ and of modes Γ_1 (Γ_2) with modes Γ_4 (Γ_3) when $\vec{X}\parallel\vec{a}'$. These effects are associated with a stress-induced admixture in wave functions but are not experimentally found. (It would result in a stress-induced activity of the silent mode Γ_2 which is opposite to the experimental finding). This justifies *a posteriori* the use of D_{4h} scattering tensors to compute the selection rules. Since Γ_3 is expected to be very sensitive to the orthorhombic distortion for $\vec{X}\parallel\vec{a}$, we note that this should result in a strong nonlinear behavior of both Γ_1 and Γ_3 modes. [Same Γ_1 symmetry in $D_{2h}(x)$.] We will come back on this point when discussing the experimental results.

Let us now concentrate on more quantitative details. The phenomenological theory of piezospectroscopic effects in rutile has been already given for electronic energy levels[9] and is basically identical for Raman-active modes. It will be simply summarized in this work. We know that the stress-induced behavior of a Raman line can be completely characterized by a set of phenomenological constants: the deformation potentials. A general description of the deformation potential approach has been given by Tekippe *et al.*[12] for α-quartz (point group D_3) and by Lemos *et al.*[10] for TeO_2 (point group D_4). To terms linear in strain, the perturbation Hamiltonian gives

$$V = V_{ij}\, e_{ij} \text{ with } i, j = x, y, z\,, \qquad (1)$$

where V_{ij} are operators which are functions of

TABLE III. Compatibility relations for the Raman-active modes in rutile under compressions $\vec{X}\parallel\vec{c}$, $\vec{X}\parallel\vec{a}$, and $\vec{X}\parallel\vec{a}$.

D_{4h} ($X=0$; $\vec{X}\parallel\vec{c}$)	Γ_1 (A_{1g})	Γ_2 (A_{2g})	Γ_3 (B_{1g})	Γ_4 (B_{2g})	Γ_5 (E_g)
$D_{2h}(x)$ ($\vec{X}\parallel\vec{a}$)	Γ_1 (A_g)	Γ_3 (B_{1g})	Γ_1 (A_g)	Γ_3 (B_{1g})	Γ_2 (B_{2g}) + Γ_4 (B_{3g})
$D_{2h}(xy)$ ($\vec{X}\parallel\vec{a}'$)	Γ_1 (A_g)	Γ_3 (B_{1g})	Γ_3 (B_{1g})	Γ_1 (A_g)	Γ_2 (B_{2g}) + Γ_4 (B_{3g})

TABLE IV. Symmetry of the products of the basis functions of Γ_5 (E_g).

	$\lvert xz\rangle$	$\lvert yz\rangle$
$\lvert xz\rangle$	$\frac{1}{2}(\Gamma_1+\Gamma_3)$	Γ_4
$\lvert yz\rangle$	Γ_4	$\frac{1}{2}(\Gamma_1-\Gamma_3)$

the undeformed coordinate system and e_{ij} are the strain components. Both V_{ij} and e_{ij} are symmetric second-rank tensors. At the Γ point of the Brillouin zone they generate the irreducible representations

$$2\Gamma_1(A_{1g})+\Gamma_3(B_{1g})+\Gamma_4(B_{2g})+\Gamma_5(E_g)\,,$$

where a given symmetry element transforms like the basis functions of the corresponding representation:

x^2+y^2 and z^2 for Γ_1 (A_{1g}),
x^2-y^2 for Γ_3 (B_{1g}),
xy for Γ_4 (B_{2g}),
xz and yz for Γ_5 (E_g) (doubly degenerated).

For rutile, and referring to the crystallographic axis, the components of the strain tensor e_{ij} are related to the components of the stress tensor X_{ij} through the elastic compliance constants S_{ij} by[13]

$$\begin{pmatrix} e_{xx}\\ e_{yy}\\ e_{zz}\\ 2e_{yz}\\ 2e_{zx}\\ 2e_{xy}\end{pmatrix}=\begin{pmatrix} S_{11} & S_{12} & S_{13} & 0 & 0 & 0\\ S_{12} & S_{11} & S_{13} & 0 & 0 & 0\\ S_{13} & S_{13} & S_{33} & 0 & 0 & 0\\ 0 & 0 & 0 & S_{44} & 0 & 0\\ 0 & 0 & 0 & 0 & S_{44} & 0\\ 0 & 0 & 0 & 0 & 0 & S_{66}\end{pmatrix}\begin{pmatrix} X_{xx}\\ X_{yy}\\ X_{zz}\\ X_{yz}\\ X_{zx}\\ X_{xy}\end{pmatrix}. \qquad (2)$$

The components of the strain tensor for $\vec{X}\parallel\vec{c}$, $\vec{X}\parallel\vec{a}$, and $\vec{X}\parallel\vec{a}'$ together with their irreducible (symmetrized) combinations have been listed in Ref. 9. Also listed are the elastic compliance constants obtained from the work of Ref. 4.

In order to get the deformation potentials in their simplest possible form we must rewrite Eq. (1) as

$$\begin{aligned} V=&\tfrac{1}{2}(V_{xx}+V_{yy})(e_{xx}+e_{yy}) && \\ &+V_{zz}e_{zz} && \Gamma_1(A_{1g})\\ &+\tfrac{1}{2}(V_{xx}-V_{yy})(e_{xx}-e_{yy}) && \Gamma_3(B_{1g})\\ &+2V_{xy}e_{xy} && \Gamma_4(B_{2g})\\ &+2V_{yz}e_{yz} && \\ &+2V_{yz}e_{zx} && \Gamma_5(E_g)\,. \end{aligned} \qquad (3)$$

The first two terms belong to Γ_1 and connect eigenfunctions with identical symmetries. They correspond to the fully symmetric part of the perturbation. The remaining terms belonging to Γ_3, Γ_4, and Γ_5; they correspond to the shear part of the perturbation.

Let us now express the stress dependence of the eigenvalue of the perturbed Hamiltonian. Consider first a nondegenerate phonon of symmetry Γ_i. In the linear regime the stress dependence is given by Γ_1 terms only and gives

$$\Delta\Gamma_i=\tfrac{1}{2}\langle\Gamma_i\,|V_{xx}+V_{yy}|\,\Gamma_i\rangle(e_{xx}+e_{yy}) +\langle\Gamma_i\,|V_{zz}|\,\Gamma_i\rangle e_{zz} \qquad (4)$$

$$=a_i(e_{xx}+e_{yy})+b_ie_{zz}\quad (i=1,3,4)\,, \qquad (5)$$

where $\Delta\Gamma_i$ is the phonon energy shift, a_i is a deformation potential associated with a pure coplanar strain perpendicular to $\vec{c}$ $(a_i=\frac{1}{2}\langle\Gamma_i\,|V_{xx}+V_{yy}|\,\Gamma_i\rangle)$, and b_i is a deformation potential associated with a pure axial strain parallel to $\vec{c}$ $(b_i=\langle\Gamma_i\,|V_{zz}|\,\Gamma_i\rangle)$.

Consider now the doubly degenerate mode Γ_5 (E_g). When $\vec{X}\parallel\vec{c}$, any linearly independent combination of eigenfunctions xz and yz forms a basis for D_{4h}. Instead, when applying a stress $\vec{X}\parallel\vec{a}$ or $\vec{X}\parallel\vec{a}'$, only one well-specified basis diagonalizes the strain Hamiltonian. In this work, we have chosen to express all coupling coefficients in the system of crystallographic eigenvectors xz and yz. They couple under application of operators whose symmetries are z^2x^2, z^2y^2, and z^2xy. The decomposition of such products in terms of the irreducible representations of D_{4h} is given in Table IV and the matrix equation gives

$$\begin{array}{cc} \lvert zx\rangle & \lvert zy\rangle \\ \left[\begin{array}{cc} a_5(e_{xx}+e_{yy})+b_5e_{zz}+c_5(e_{xx}-e_{yy}) & d_5e_{xy}\\ d_5e_{xy} & a_5(e_{xx}+e_{yy})+b_5e_{zz}-c_5(e_{xx}-e_{yy})\end{array}\right] \end{array}, \qquad (6)$$

with

$$a_5 = \tfrac{1}{4}\langle f_0' | V_{xx} + V_{yy} | f_0' \rangle ,$$
$$b_5 = \tfrac{1}{2}\langle \psi_0' | V_{zz} | \psi_0' \rangle ,$$
$$c_5 = \tfrac{1}{4}\langle f_1' | V_{xx} - V_{yy} | f_1' \rangle ,$$
$$d_5 = 2\langle f_2' | V_{xy} | f_2' \rangle .$$

Of course, with this representation the nondiagonal part corresponds to a pure stress $\vec{X} \parallel \vec{a}'$; the situation would be reversed in representation zx', zy'. The parameters a_5 and b_5 are fully symmetric deformation potentials, while c_5 and d_5 are pure shear deformation potentials. f_0', ψ_0', f_1', and f_2' are the basis functions listed in Table I for representations Γ_1 (A_{1g}), Γ_3 (B_{1g}), and Γ_4 (B_{2g}), respectively.

The resulting eigenvalues are

$$\Delta\Gamma_5 = a_5(e_{xx} + e_{yy}) + b_5 e_{zz} + [c_5^2(e_{xx} - e_{yy})^2 + d_5^2 e_{xy}^2]^{1/2} . \tag{7}$$

For stresses directed along the crystal $\vec{c}$, $\vec{a}$, and $\vec{a}'$ axes, respectively, application of Eqs. (5) and (7), together with the deformations listed in Ref. 9, gives the slope parameters listed in Table V. For a nondegenerate phonon, we get two independent parameters (a_i, b_i) and three independent determinations. For the doubly degenerate Γ_5 mode, we get four independent parameters and five independent slopes. We expect again the fully symmetric part to be identical for $\vec{X} \parallel \vec{a}$ and $\vec{X} \parallel \vec{a}'$.

III. EXPERIMENTAL DETAILS

The Raman spectrometer used in this experiment was made of a Spectra Physics Model 165 Ar^+-ion laser, a Coderg T800 triple monochromator, and a cooled EMI 9816 QA photomultiplier. A right-angle scattering geometry and conventional lock-in detection techniques were used. The Raman spectra were recorded with typically 400 mW of the 5145-Å laser line and a spectral resolution below 1 cm^{-1}.

The stressing apparatus is shown in Fig. 2. It is designed to work at room temperature and is small enough (15×15 cm^2) to render the alignment procedure simple. It is made of two optically flat pistons (2, 3) with sample (1) compressed in between. Piston (3) is fixed and is drilled with a small aperture (~1.5 mm diam) which allows the incident light to impinge upon the sample. In this configuration the full length of the sample was used in 90° scattering experiment and could be focused on the horizontal entrance slit of our monochromator. A transparent glass window (4) is positioned between the sample and piston (2). A quartz-force transducer (5) controls the strength. Piston (2) is allowed to move. Its displacement is driven by the small rotation of the left arm (6) of a deformable fork (7). It can be modified by tightening the screw (8) working against a spring.

All TiO_2 samples used in this experiment were x ray oriented from a single ingot.[14] They were in the form of small parallelepipeds approximately $10 \times 1 \times 1$ mm^3 and, in order to ensure a better stress homogeneity, all small pressure faces were optically flat. Three different configurations have been used. First, the long dimension (direction of the stress and of the incident light) was along $\vec{c}$ (or $\vec{a}$), then the scattered light was collected along $\vec{a}$ (or $\vec{c}$). Second, the long dimension was along $\vec{a}'$ (x' axis) and the scattered light was collected along $\vec{c}$. In both cases, by rotating the polarization of the incident light, we could observe all Raman-active modes through the xy ($x'y'$), zx (zx'), zy (zy'), and y^2 (y'^2) components of the scattering tensors listed in Table II for the rectangular (and 45°) cut.

IV. EXPERIMENTAL RESULTS AND DISCUSSION

A zero-stress Raman spectrum is shown in Fig. 3. We note the phonon frequencies, Γ_3 (B_{1g}) ap-

TABLE V. Stress dependence $d\Gamma_i/dX$ of the most important Raman-active modes of TiO_2.

	$\vec{X} \parallel \vec{c}$	$\vec{X} \parallel \vec{a}$	$\vec{X} \parallel \vec{a}'$
Γ_1 (A_{1g})	$2a_1S_{13} + b_1S_{33}$	$a_1\ (S_{11} + S_{12}) + b_1S_{13}$	$a_1\ (S_{11} + S_{12}) + b_1S_{13}$
612 cm^{-1}	0.11 ± 0.04 cm^{-1}/kbar	0.10 ± 0.04 cm^{-1}/kbar	0.11 ± 0.04 cm^{-1}/kbar
Γ_3 (B_{1g})	$2a_3S_{13} + b_3S_{33}$	$a_3\ (S_{11} + S_{12}) + b_3S_{13}$	$a_3\ (S_{11} + S_{12}) + b_3S_{13}$
143 cm^{-1}	$+0.02 \pm 0.02$ cm^{-1}/kbar	-0.13 ± 0.02 cm^{-1}/kbar	-0.16 ± 0.02 cm^{-1}/kbar
Γ_4 (B_{2g})	$2a_4S_{13} + b_4S_{33}$	$a_4\ (S_{11} \pm S_{12}) + b_4S_{13}$	$a_4\ (S_{11} + S_{12}) + b_4S_{13}$
826 cm^{-1}	...	...	...
Γ_5 (E_g)	$2a_5S_{13} + b_5S_{33}$	$a_5\ (S_{11} + S_{12}) + b_5S_{13} \pm c_5(S_{11} - S_{12})$	$a_5\ (S_{11} + S_{12}) + b_5S_{13} \pm \frac{1}{4}d_5S_{66}$
449 cm^{-1}	0.28 ± 0.04 cm^{-1}/kbar	$\begin{cases} 0.21 \pm 0.04\ \text{cm}^{-1}/\text{kbar} \\ 0.13 \pm 0.04\ \text{cm}^{-1}/\text{kbar} \end{cases}$	$\begin{cases} 0.20 \pm 0.04\ \text{cm}^{-1}/\text{kbar} \\ 0.14 \pm 0.04\ \text{cm}^{-1}/\text{kbar} \end{cases}$

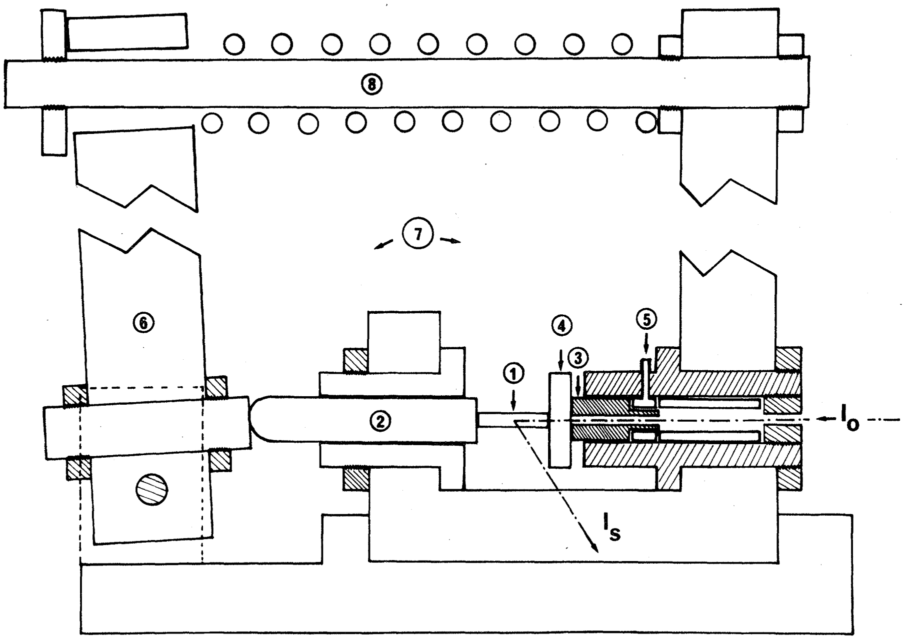

FIG. 2. Schematic drawing of the room-temperature stressing apparatus. The incident light (I_0) impinges upon sample (1) through a small aperture drilled in the fixed piston (3). Piston (2) is allowed to move and its displacement is controlled by the small rotation of the left arm (6) of the deformable fork (7). (4) is a quartz window, (5) a quartz transducer, and (8) is a screw working against a spring. The scattered intensity I_s is collected in 90° scattering geometry.

pearing first at 143 cm^{-1}. Γ_5 (E_g) is found at 450 cm^{-1}, Γ_1 (A_{1g}) at 612 cm^{-1}, and, last, Γ_4 (B_{2g}) at 826 cm^{-1}. All values are in good agreement with previously published data.[1,5] We note the very weak scattering intensity associated with the Γ_4 mode: It precludes any attempt to deduce accurately the corresponding stress dependence. Also the strong two-phonon band[1] which appears near 235 cm^{-1} was not investigated.

A. Γ_3 (B_{1g}) mode at 143 cm^{-1}

This is the sharpest mode of the Raman spectrum of TiO_2. The experimental linewidth which is about 2 cm^{-1} permits rather accurate measurements. The results are displayed in Figs. 4(a) ($\vec{X}\parallel\vec{c}$) and 5(a) ($\vec{X}\parallel\vec{a}$ and $\vec{X}\parallel\vec{a}'$), respectively. First we note that the Γ_3 mode behavior is found normal in configuration $\vec{X}\parallel\vec{c}$, i.e., the phonon frequency increases under uniaxial compression. However, the magnitude of the displacement is extremely small and cannot compensate for the strong softening observed when $\vec{X}\parallel\vec{a}$ or $\vec{X}\parallel\vec{a}'$ [see Fig. 5(a)]. This effect results in the soft-mode behavior already reported under hydrostatic conditions.[5,6]

As already said, our results in configuration $\vec{X}\parallel\vec{c}$ disagree with the experimental findings of Ref. 11 (see Table VI). We get almost identical absolute values but opposite signs. However, it should be noted in both cases that the experimental shift appears very small and in fact is of the order of the experimental uncertainty. So the disagreement may not be very significant. It should be noted also that different shapes have been used for the samples: $3.5\times3.5\times1.5$ mm^3 in Ref. 11 against $10\times1\times1$ mm^3 in the work. A small amount of nonuniaxial component which may be present with the square samples would be sufficient to turn the uniaxial-stress dependence from positive in configuration $\vec{X}\parallel\vec{c}$ (according to our data) to slightly negative because of an $\vec{X}\parallel\vec{c}$ and $\vec{X}\parallel\vec{a}$ admixture.

The solid curves in Figs. 4 and 5 are least-squares fits through the experimental data. Con-

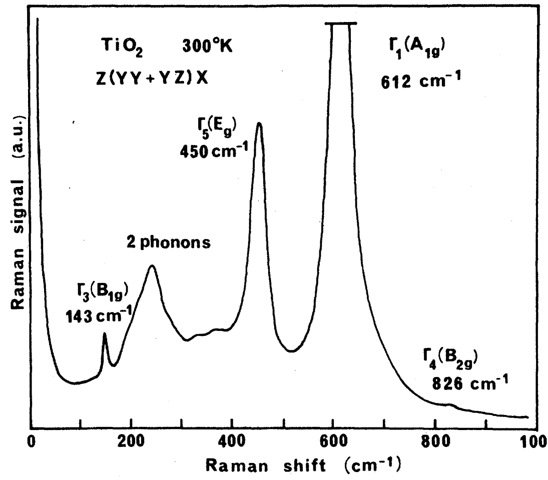

FIG. 3. Zero-stress Raman spectrum. The $\Gamma_3(B_{1g})$ mode appears at 143 cm^{-1}, Γ_5 (E_g) at 450 cm^{-1}, Γ_1 (A_{1g}) at 612 cm^{-1}, and $\Gamma_4(B_{2g})$ at 826 cm^{-1}. The strong feature near 235 cm^{-1} is a two-phonon band.

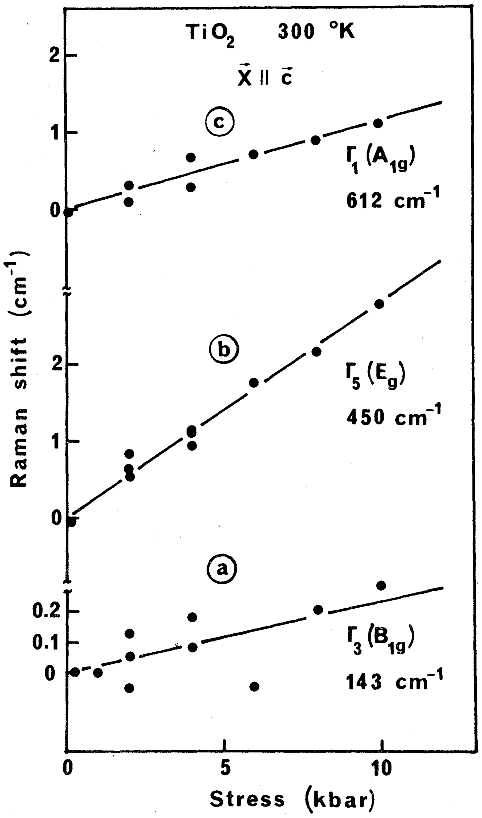

FIG. 4. (a) Stress dependence of Γ_3 (B_{1g}) in configuration $\vec{X} \parallel \vec{c}$. The solid line is a least-mean-squares fit through the experimental data with slope 0.02 ± 0.02 cm^{-1}/kbar. Note the scale on the vertical axis. (b) Same as Fig. 1(a) but for Γ_5 (E_g). The best fit gives a slope 0.28 ± 0.04 cm^{-1}/kbar. (c) Same as Fig. 1(a) but for Γ_1 (A_{1g}). The slope is 0.11 ± 0.04 cm^{-1}/kbar.

cerning Γ_3 (B_{1g}), they give the slopes

$\vec{X} \parallel \vec{c}$: $+(0.02 \pm 0.02)$ cm^{-1}/kbar ,

$\vec{X} \parallel \vec{a}$: $-(0.13 \pm 0.02)$ cm^{-1}/kbar ,

$\vec{X} \parallel \vec{a}'$: $-(0.16 \pm 0.02)$ cm^{-1}/kbar .

Using the theoretical expressions of Table V and the S_{ij} parameters listed in Ref. 9, we deduce two deformation potentials, a_3 and b_3, associated with the Γ_3 phonon mode. In units of cm^{-1}, we get

$$a_3 = 620 \pm 120 \text{ cm}^{-1} \text{ and } b_3 = 330 \pm 120 \text{ cm}^{-1} .$$

To compare with previous experiments, we must deduce from our data the frequency shift associated with pure hydrostatic conditions. Introducing the deformations

$$e_{xx} = (S_{11} + S_{12} + S_{13})P = e_{yy} , \quad e_{zz} = (2S_{13} + S_{33})P ,$$

we get

$$\frac{d\Gamma_3}{dP} = 2a_3(S_{11} + S_{12} + S_{13}) + b_3(2S_{13} + S_{33}) ,$$

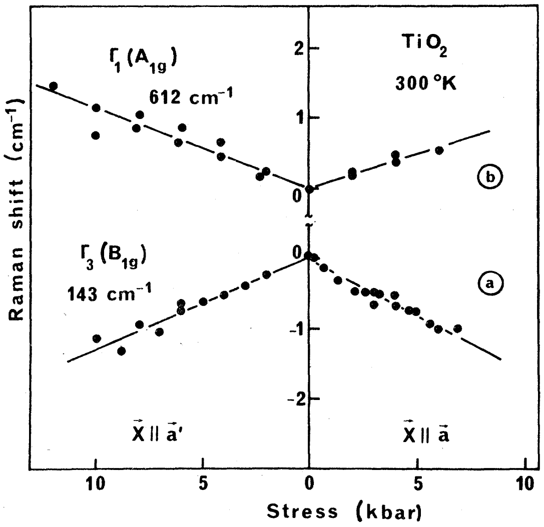

FIG. 5. (a) Stress dependence of the low-frequency Γ_3 (B_{1g}) mode in configuration $\vec{X} \parallel \vec{a}$ and $\vec{X} \parallel \vec{a}'$. Note the negative dependence. The solid lines are least-mean-squares fits which give the slopes $-(0.13 \pm 0.02)$ cm^{-1}/kbar in configuration $\vec{X} \parallel \vec{a}$ and $-(0.16 \pm 0.02)$ cm^{-1}/kbar in configuration $\vec{X} \parallel \vec{a}'$. (b) Same as (a) but for Γ_1(A_{1g}). Note the positive stress dependences (normal mode behavior). The solid lines give 0.10 ± 0.04 cm^{-1}/kbar ($\vec{X} \parallel \vec{a}$) and 0.11 ± 0.04 cm^{-1}/kbar ($\vec{X} \parallel \vec{a}'$).

which gives in the notation of Table V

$$\frac{d\Gamma_3}{dP} = 2\left(\frac{d\Gamma_3}{dX}\right)_{\vec{X} \parallel \vec{a}} + \left(\frac{d\Gamma_3}{dX}\right)_{\vec{X} \parallel \vec{c}} .$$

From our experimental results we get a pressure coefficient $d\Gamma_3/dP = -(0.24 \pm 0.06)$ cm^{-1}/kbar to be compared with the experimental results of Ref. 5: $-(0.34 \pm 0.03)$ cm^{-1}/kbar; Ref. 6: -0.36 cm^{-1}/kbar; and Ref. 11: $-(0.37 \pm 0.07)$ cm^{-1}/kbar. Within experimental uncertainty, all results are in satisfactory agreement and support an average value: $-(0.33 \pm 0.05)$ cm^{-1}/kbar.

The mode Grüneisen parameter γ_3 can also be extracted from the deformation potentials a_3 and b_3:

$$\gamma_3 = -\frac{d(\ln\Gamma_3)}{d(\ln V)} = -\frac{1}{\Gamma_3}\,\frac{a_3 + kb_3}{1 + k} ,$$

with

$$k = \frac{1}{2}\,\frac{2S_{13} + S_{33}}{S_{11} + S_{12} + S_{13}} .$$

We get $\gamma_3 = -(4 \pm 1)$ to be compared with $\gamma_3 = -5$ in Ref. 5.

Within experimental error, the least-mean-squares fit gives identical slopes for Γ_3 in configurations $\vec{X} \parallel \vec{a}$ and $\vec{X} \parallel \vec{a}'$, and we do not find the nonlinear behavior expected in configuration $\vec{X} \parallel \vec{a}$. This point is worth noting. It shows that Γ_3 (B_{1g}) does not exhibit the special sensitivity to the orthorhombic distortion previously sugges-

TABLE VI. Summary of the uniaxial-stress dependences and hydrostatic pressure coefficients reported for TiO_2. When measured from the uniaxial-stress experiments, the hydrostatic pressure coefficients were deduced from equation $d\Gamma_i/dP = d\Gamma_i/dX|_{\vec{X}\parallel\vec{c}} + 2d\Gamma_i/dX|_{\vec{X}\parallel\vec{a}}$.

	$d\Gamma_i/dX$ (cm^{-1}/kbar)				Average value
	a	b	c	d	
Γ_1	$\vec{X}\parallel\vec{c}$ 0.11 ± 0.04				
(A_{1g})	$\vec{X}\parallel\vec{a}$ 0.10 ± 0.04	0.24 ± 0.06			0.17 ± 0.05
612 cm^{-1}	$\vec{X}\parallel\vec{a}'$ 0.11 ± 0.04				
	hydrostatic component 0.31 ± 0.12		0.41	0.46 ± 0.12	0.39 ± 0.12
Γ_3	$\vec{X}\parallel\vec{c}$ 0.02 ± 0.02	−0.03 ± 0.01			−0.01 ± 0.02
(B_{1g})	$\vec{X}\parallel\vec{a}$ −0.13 + 0.02	−0.17 ± 0.03			−0.15 ± 0.03
143 cm^{-1}	$\vec{X}\parallel\vec{a}'$ −0.16 + 0.02				
	hydrostatic component −0.24 + 0.06	−0.37 ± 0.07	−0.36	−0.34 ± 0.03	−0.33 ± 0.05
Γ_5	$\vec{X}\parallel\vec{c}$ 0.28 ± 0.04	0.18 ± 0.04			0.23 ± 0.04
(E_g)	$\vec{X}\parallel\vec{a}$ $\begin{cases}0.21 + 0.04\\0.13 + 0.04\end{cases}$	0.18 + 0.04[e]			0.18 ± 0.06[e]
449 cm^{-1}	$\vec{X}\parallel\vec{a}'$ $\begin{cases}0.20 + 0.04\\0.14 + 0.04\end{cases}$				
	hydrostatic component 0.62 + 0.12	0.54 + 0.12	0.43	0.52 + 0.09	0.53 + 0.11

[a] This work.
[b] Reference 11.
[c] Reference 6.
[d] Reference 5.
[e] Center of gravity; the two components of the stress-induced doublet were not resolved in the work of Ref. 11.

ted. In fact the atomic displacements for this vibrational mode correspond with pure rotations of the oxygen atoms around the central titanium atom. Such rotations are associated with a bending of the first-nearest-neighbor interactions. In the following paper it will be shown that the stress-induced change in the bond-bending constants results in a normal softening of the Γ_3 Raman mode.

B. $\Gamma_1(A_{1g})$ mode at 612 cm^{-1}

This is the strongest mode of the Raman spectrum in Fig. 3. The spectral line is rather broad and the accuracy in the peak position is only ±0.2 cm^{-1}. In configuration $\vec{X}\parallel\vec{c}$, the stress dependence is displayed in Fig. 4(b). In Fig. 5(b) it is displayed for configurations $\vec{X}\parallel\vec{a}$ and $\vec{X}\parallel\vec{a}'$. From the least-squares fits (solid curves) we get the slope coefficients

$$\vec{X}\parallel\vec{c}: +(0.11 \pm 0.04)\ \mathrm{cm^{-1}/kbar},$$

$$\vec{X}\parallel\vec{a}: +(0.10 \pm 0.04)\ \mathrm{cm^{-1}/kbar},$$

$$\vec{X}\parallel\vec{a}': +(0.11 \pm 0.04)\ \mathrm{cm^{-1}/kbar}.$$

Within experimental error, all pressure coefficients are identicals. The deformation potentials and mode Grüneisen parameter deduced from the measurements are $a_1 = -(610 \pm 240)$ cm^{-1}, $b_1 = -(820 \pm 310)$ cm^{-1}, and $\gamma_1 = +(1 \pm 0.4)$. We find negative signs for the deformation potentials and a positive sign for the mode Grüneisen parameter. This reflects the normal mode behavior of Γ_1: The phonon frequency stiffens versus pressure. In the next paper it will be shown that this is an effect of the stress-induced change in the bond-stretching constants between first-nearest neighbors.

The mode Grüneisen parameter found in this work (1 ± 0.4) appears slightly lower than the value quoted in Ref. 5 from hydrostatic experiments ($\gamma_1 = 1.6$). Also the hydrostatic pressure coefficient

$$\frac{d\Gamma_1}{dP} = 0.31 \pm 0.12\ \mathrm{cm^{-1}/kbar}$$

appears slightly lower than the values 0.46 ± 0.12 cm^{-1}/kbar quoted in Ref. 5 and 0.41 cm^{-1}/kbar quoted in Ref. 6. The discrepancy however stays within the experimental uncertainty and supports an average value (0.39 ± 0.12) cm^{-1}/kbar.

C. Γ_5 (E_g) mode (450 cm^{-1})

This is the only doubly degenerate mode of the Raman spectrum. It has been identified[1] at 450 cm^{-1}. In Fig. 3, the corresponding spectral line is again very broad (~30 cm^{-1}) and the experimental accuracy in pointing the peak maximum is 0.2 cm^{-1}. The line splits under compressions $\vec{X} \parallel \vec{a}$ and $\vec{X} \parallel \vec{a}'$ according to the compatibility relations listed in Table III. In configuration $\vec{X} \parallel \vec{a}$, the two split components Γ_2 and Γ_4 correspond to the nondiagonal part α_{zx} and α_{zy}, respectively, of the polarizability tensors listed in Table II. Their energy separation is achieved by use of their polarization properties. We work in configuration $\langle x|zx|z\rangle$ to resolve the Γ_2 (B_{2g}) component and in configuration $\langle x|zy|z\rangle$ to resolve Γ_4 (B_{3g}). The same is true for $\vec{X} \parallel \vec{a}'$, but with x' and y' replacing x and y, respectively (45° cut of the sample).

For stresses directed along the crystal $\vec{c}$ axis, the mode frequency shifts and remains degenerate. This is shown in Fig. 4(c). From the least-mean-squares fit, we get a positive slope 0.28 ± 0.04 $\text{cm}^{-1}/\text{kbar}$.

For stresses parallel to $\vec{a}$, the phonon frequency shifts and splits as shown in Fig. 6(a). Similar results are obtained in direction $\vec{X} \parallel \vec{a}'$. They are shown in Fig. 6(b). For clarity we display on separate scales the four components. It is interesting to note that the Γ_4 mode, which is the high-energy mode (hard component) for $\vec{X} \parallel \vec{a}$, becomes the soft component for $\vec{X} \parallel \vec{a}'$. This behavior can be qualitatively understood in light of the deformations and atomic displacements shown in Fig. 7. For $\vec{X} \parallel \vec{a}$, the crystal structure reduces to $D_{2h}(x)$ and a group theory analysis shows that the Γ_2 (B_{2g}) mode corresponds to an out-of-phase vibration of the pairs of oxygen atoms characterized by a shorter bond length. This increased coupling between the pairs of neighboring atoms beating out of phase in the $\vec{c}$ direction results in a quenching of the vibration, i.e., in a softening of the mode. Conversely, for the Γ_4 (B_{3g}) mode, the coupling between pairs of neighboring atoms which beat in phase increases, and this hardens the mode with respect to Γ_2. For $\vec{X} \parallel \vec{a}'$, only one pair of oxygen atoms beat, the two atoms having out-of-phase displacements. The other pair of atoms is at rest. If the coupling between the two beating atoms increases, the frequency hardens. This corresponds to Γ_4 (B_{3g}). If the coupling between the two beating atoms decreases, the mode fre-

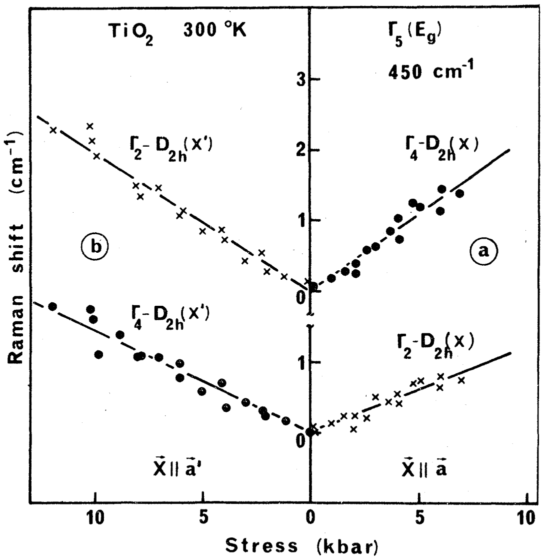

FIG. 6. (a) Stress dependence of the two Γ_5 (E_g) split modes in configuration $\vec{X} \parallel \vec{a}$. For convenience the two components are displayed on separate scales. The solid lines are again least-mean-squares fits through the experimental data. They give the slopes 0.21 ± 0.04 $\text{cm}^{-1}/\text{kbar}$ for Γ_4 mode and 0.13 ± 0.04 $\text{cm}^{-1}/\text{kbar}$ for Γ_2 mode. (b) Same as (a) but for $\vec{X} \parallel \vec{a}'$. The slopes are 0.20 ± 0.04 $\text{cm}^{-1}/\text{kbar}$ for Γ_2 and 0.14 ± 0.04 $\text{cm}^{-1}/\text{kbar}$ for Γ_4. Γ_2 components are found in polarization α_{xz} ($\alpha_{x'z}$) and Γ_4 components in polarization α_{yz} ($\alpha_{y'z}$), respectively.

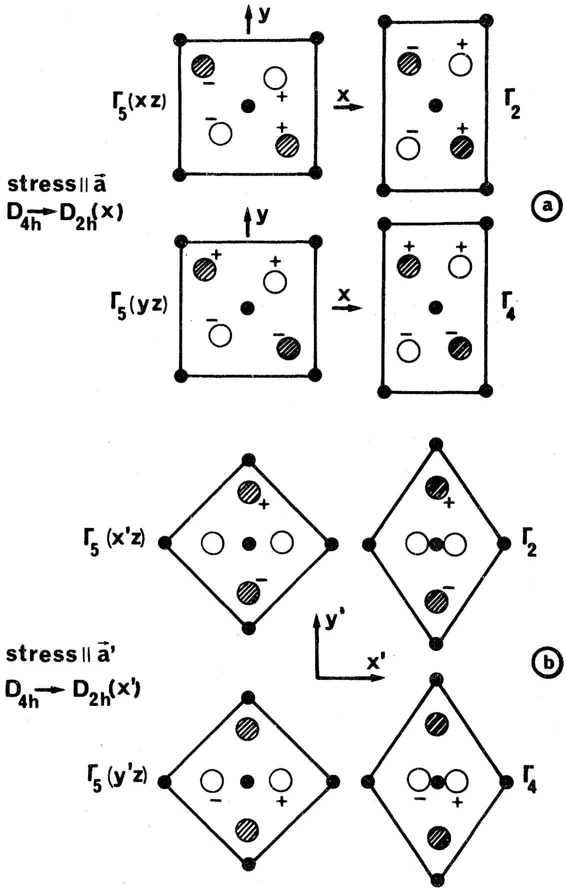

FIG. 7. Atomic displacements for the doubly degenerate Γ_5 mode: (a) stress parallel to $\vec{a}$, (b) stress parallel to $\vec{a}'$. In both cases, the hard component is associated with an increased separation between the pair of atoms which beat out of phase. This is Γ_4 for $\vec{X} \parallel \vec{a}$ and Γ_2 for $\vec{X} \parallel \vec{a}'$.

quency softens. This corresponds to Γ_2 (B_{2g}).

From the least-mean-squares fit, we get the slopes of the four phonon branches. They are 0.21 ± 0.04 cm^{-1}/kbar and 0.13 ± 0.04 cm^{-1}/kbar for compressions $\vec{X} \parallel \vec{a}$, and 0.20 ± 0.04 cm^{-1}/kbar and 0.14 ± 0.04 cm^{-1}/kbar for $\vec{X} \parallel \vec{a}'$. Within experimental error, the splitting appears identical in both configurations and indicates an isotropic behavior of the doubly degenerate Γ_5 mode under compressions perpendicular to $\vec{c}$. No comparison is possible with the work of Ref. 11 in which the splitting was not resolved in configuration $\vec{X} \parallel \vec{a}$.

In good agreement with the theoretical results on Table V, the fully symmetric Γ_1 part of the interaction is identical for both directions. We find a slope

$$\left(\frac{d\Gamma_5}{dX}\right)_{\Gamma_1} = a_5(S_{11}+S_{12}) + b_5 S_{13}$$

$$= 0.17 \pm 0.08 \text{ cm}^{-1}/\text{kbar} .$$

From this result, together with the slope obtained with $\vec{X} \| \vec{c}$, we get $a_5 = -(1170 \pm 370)$ cm^{-1}, $b_5 = (-1840 \pm 430)$ cm^{-1}, $\gamma_5 = +(2.9 \pm 0.9)$ cm^{-1}.

Again the mode Grüneisen parameter obtained for uniaxial-stress experiments appears in satisfactory agreement with the one obtained from hydrostatic measurements[5]: $\gamma_5 = 2.43$. The hydrostatic pressure coefficient obtained from our data is 0.62 ± 0.12 cm^{-1}/kbar to be compared with 0.52 ± 0.09 in Refs. 5, 0.43 in Ref. 6, and (0.54 ± 0.13) cm^{-1}/kbar in Ref. 11. All results support an average value: $0.53 + 0.11$ cm^{-1}/kbar.

The shear deformation potentials deduced from the measurements are $c_5 = +(35 \pm 35)$ cm^{-1} and $d_5 = -(230 \pm 300)$ cm^{-1}. The sign is positive for c_5 and negative for d_5. This comes from the selection rules indicated in Fig. 6: The soft component has symmetry for $\vec{X} \parallel \vec{a}$ and zy' symmetry for $\vec{X} \parallel \vec{a}'$.

V. CONCLUSION

We have investigated the effect of static uniaxial compressions on the first-order Raman spectrum of TiO_2. All uniaxial-stress dependences obtained in this work are summarized in Table VI. The comparison with previously published data shows minor discrepancies which stay in the limit of the experimental uncertainty. We have found linear displacements of the two nondegenerate modes Γ_1 and Γ_3 associated with the following deformation potentials:

$$a_1 = -(610 \pm 240) \text{ cm}^{-1}, \quad b_1 = -(820 \pm 310) \text{ cm}^{-1},$$

$$a_3 = +(620 \pm 120) \text{ cm}^{-1}, \quad b_3 = +(330 \pm 150) \text{ cm}^{-1}.$$

In configuration $\vec{X} \parallel \vec{a}$, the linear behavior of Γ_3 versus deformation rules out a peculiar sensitivity of this Raman mode to the orthohombic distortion. In fact, the positive deformation potentials which are found in this case reflect the change in bond-bending constants versus deformation. This will be shown in the following paper.

The doubly degenerate Γ_5 mode shifts and splits, under stress parallel to $\vec{a}$ and parallel to $\vec{a}'$. The four deformation potentials which are found in this case are

$$a_5 = -(1170 \pm 370) \text{ cm}^{-1}, \quad b_5 = -(1840 \pm 430) \text{ cm}^{-1},$$

$$c_5 = +(35 \pm 35) \text{ cm}^{-1}, \quad d_5 = -(230 \pm 300) \text{ cm}^{-1}.$$

ACKNOWLEDGMENT

We greatly thank L. Martin for expert assistance with the Raman spectrometer.

---

*Present address: Departament d'Electricitat i Electrònica, Universitat Autònoma, Bellaterra, Barcelona, Spain.

†Centre associé au CNRS.

[1] S. P. S. Porto, P. A. Fleury, and T. C. Damen, Phys. Rev. 154, 522 (1967).

[2] W. G. Spitzer, R. C. Miller, D. A. Kleinman, and L. E. Howarth, Phys. Rev. 126, 1710 (1962).

[3] J. G. Traylor, H. G. Smith, R. M. Nicklow, and M. K. Wilkinson, Phys. Rev. B 3, 3457 (1971).

[4] M. H. Grimsditch and A. K. Ramdas, Phys. Rev. B 14, 1670 (1976).

[5] G. A. Samara and P. S. Peercy, Phys. Rev. B 7, 1131 (1973).

[6] M. Nicol and M. Y. Fong, J. Chem. Phys. 54, 3167 (1971).

[7] L. Nagel and M. O'Keeffe, Mater. Res. Bull. 6, 1317 (1971).

[8] A. E. Austin, J. Phys. Chem. Solids, 30, 1282 (1969).

[9] H. Mathieu, J. Pascual, and J. Camassel, Phys. Rev. B 18, 6920 (1978).

[10] V. Lemos, F. Cerdeira, M. A. F. Scarparo, and R. S. Katiyar, Phys. Rev. B 16, 5560 (1977).

[11] P. S. Peercy, Phys. Rev. B 8, 6018 (1973).

[12] V. J. Tekippe, A. K. Ramdas, and S. Rodriguez, Phys. Rev. B 8, 706 (1973).

[13] See, for example, J. F. Nye, *Propriétés physiques des Cristaux* (Dunod, Paris, 1971).

[14] S. A. Djevahirdjian, 1870 Monthey (Valais) Switzerland.